IEEE Access
Multidisciplinary ⋮ Rapid Review ⋮ Open Access Journal

Received 28 May 2024, accepted 12 June 2024, date of publication 17 June 2024, date of current version 24 June 2024.

Digital Object Identifier 10.1109/ACCESS.2024.3415381

RESEARCH ARTICLE

Robust Object Tracking Against Sensor Failures With Centralized IMM Filter

JAEHO CHOI[1], JONGWON PARK[1], AND KUNSOO HUH[2], (Member, IEEE)
[1]Department of Automotive Engineering (Automotive-Computer Convergence), Hanyang University, Seoul 04763, Republic of Korea
[2]Department of Automotive Engineering, Hanyang University, Seoul 04763, Republic of Korea

Corresponding author: Kunsoo Huh (khuh2@hanyang.ac.kr)

This work was supported by the Ministry of Trade, Industry, and Energy (MOTIE), South Korea, through the Technology Innovation Program (Development on Automated Driving With Perceptual Prediction Based on T-Car/Vehicle Parts to Intelligent Control/System Integration for Assessment) under Grant 20018101.

ABSTRACT Highly automated driving requires the use of multiple sensors for reliable tracking functionality. In response to the requirement, the proposed method modifies the conventional Interacting Multiple Model (IMM) filter to fuse multi-sensor data by utilizing the independence of observations. In addition, the proposed IMM is integrated with a Centralized Kalman Filter (CKF) that ensures track continuity against sensor failures, providing optimal state estimates. When tracking objects in a moving reference frame, such as in autonomous vehicles, onboard sensor measurements represent relative values, making it challenging to estimate the actual motion of objects. While transforming states to a global coordinates is a solution, the solution can arise another problem where the tracking results depends on the status and performance of the localization. Therefore, to tackle the problem, a track compensation algorithm utilizing a hybrid coordinate system is proposed. The actual motions of objects are estimated based on errors between the track state and the associated measurement. The performance of the proposed algorithms is demonstrated using experimental scenario data conducted with an actual vehicle.

INDEX TERMS Interacting multiple model filter, multi-sensor system, sensor failure, sensor fusion, state estimation.

I. INTRODUCTION

Recent advancements in autonomous vehicle technology have increased the demand for reliable perception performance. This is evident because autonomous vehicles need to be aware of their surroundings and establish effective control strategies. In particular, highly automated driving systems are required to perform various Object and Event Detection and Response (OEDR) tasks [1]. Among environmental sensors, RAdio Detection and Ranging (RADAR), Light Detection and Ranging (LiDAR), and cameras can be used in vehicles to recognize their surroundings, and the data from these sensors needs to be processed to detect objects and obstacles. As a result, various processing methods for each sensor have been studied to enhance the reliability of perception systems. Among these studies, camera-based and LiDAR-based object detection have gained significant attention due to their excellent performance.

However, it has been reported that relying solely on one type of sensor may have limitations such as deteriorated detection performance in weather conditions. A single-sensor system cannot sufficiently meet the requirements of highly automated driving. Hence, it is essential to establish robust perception capabilities using multiple sensors. There are ongoing efforts to fuse data from multiple sensors to develop complementary perception algorithms, which is referred to as sensor fusion. This paper specifically focuses on the high-level fusion system for object tracking.

In the field of object tracking, there have been studies aimed at improving accuracy and reducing computational load. According to [2], [3], [4], [5], [6], and [7], studies on high-level data processing consist of multi-sensor data fusion, data association, track management, and state estimation.

Sensor fusion systems can take various forms depending on the type of sensor data and the fusion structure.

The associate editor coordinating the review of this manuscript and approving it for publication was Chih-Yu Hsu.

In terms of the structure, they can be classified into two categories: distributed and centralized as depicted in Fig. 1. The distributed structure has independent state estimators and creates separate tracks for each sensor. Traditionally, distributed structures have been preferred for their computational efficiency and mathematical convenience. Besides, they have a clear sequence such as state estimation and weighted combination. On the other hand, the centralized structure is mathematically complex and computationally expensive. However, it has a single estimator structure that allows for easy parameters adjustment, and avoids error accumulation and uncertainty from a separate weighted combination process.

The data association algorithm is responsible for establishing the relationship between the estimated track states and measurements from sensors. Depending on the specific method employed, association results can be represented as either a joint probability or an event tree. Track management performs the initialization and termination of tracks. From the association information, the manager terminates tracks with low existence probabilities while maintaining those with high probabilities, thus enabling their utilization for path prediction and decision making.

To provide the states of surrounding objects for subsequent steps such as path prediction and decision making, accurate estimation of the track state is required. For example, Kalman filters have been commonly used for this purpose due to their ease of implementation and ability to achieve accuracy. But, the standard Kalman filter (KF) [8] has a limitation that they are designed to work with only a single motion model.

In particular, for automated driving, it is difficult to track objects accurately with a single motion model because there exist numerous objects with various types of motions. In order to address this problem, Interacting Multiple Model (IMM) techniques [9], [10] have been developed with integrating estimates from multiple models. However, data fusion from multiple sensors with the IMM is challenging due to its formulation. Because the equations for the model interaction and mode probability update step of the IMM filter are not applicable to multi-sensor systems.

To address the limitations of the IMM filter in multi-sensor object tracking applications, a centralized fusion formula was utilized. The Centralized KF (CKF) and IMM are employed to fuse multi-sensor data for estimating the state and covariance information of objects. Approaches of the Weighted Least Squares (WLS) [11], the Information Filter (IF) [12], and the Sequential Least Squares (SLS) [13] are utilized, assuming a Gaussian distribution of the sensor's detection. This assumption makes it possible to estimate mean and variance without requiring knowledge of the Probability Density Function (PDF) of the sensor detection model. Since the sufficient statistics are known or adjustable in this application, IF and SLS can be integrated with the IMM. Then, the CKF is applied to the IMM filter based on the independence of the observation events. To perform sensor fusion with IMM filter, it is necessary to modify the

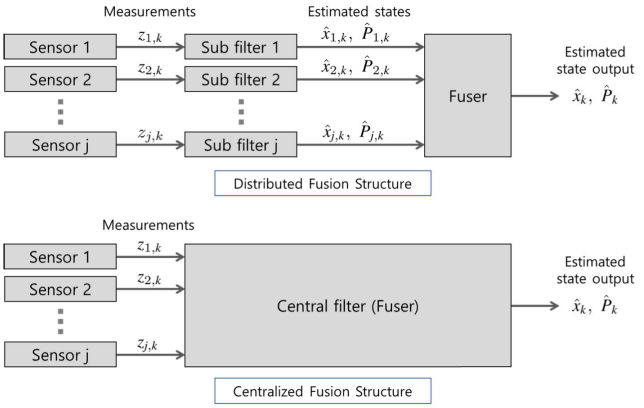

FIGURE 1. Sensor fusion structures.

equations of the KF, which is the sub-filter of the IMM filter. The CKF is utilized instead of Distributed KF (DKF) because centralized fusion outperforms distributed fusion in terms of optimality and track continuity. The suggested algorithm has high flexibility because the formulation remains unaffected by changes in the number of sensors. Thus, this enables it to handle sensor failure scenarios effectively.

A failure in one or more sensors can cause incorrect data being fed into the fusion algorithm, potentially degrading the tracking functionality. Failures can originate from various sources, such as mechanical breakdowns in sensors, communication loss between sensors and the processing unit, and bad weather conditions such as fog and heavy rain [14]. Failures not only degrade the object tracking performance, but also jeopardize driving safety due to incorrect tracking results. To address these limitations, various sensor fusion algorithms have been developed that can detect failures [15] and compensate for compromised sensor data [16].

The perception system selects either a global coordinate system or a moving coordinate (reference) system to perform object tracking. When selecting the global coordinate system, tracking objects becomes impossible if GPS is not installed or its signals are unavailable [17]. In highly automated driving, such as level 4 and above, it is necessary to maintain object tracking functionality even in situations where GPS is not operational [1]. Therefore, selecting the global coordinates for tracking can be a risk to systems that require stable functionality, such as highly automated driving.

In this study, object tracking is investigated in the moving reference frame. Selecting a moving reference frame offers an advantage of less computational burden and it yields smaller errors in object tracking compared to those of the global coordinate system [18]. However, since this selection induces relative quantities in sensor measurements, it is not easy to estimate the actual motion of objects accurately when mode matched filtering algorithms are utilized such as the IMM. Thus, track compensation algorithm is proposed which compensates the state of an object with the amount of host vehicle's movement. With the proposed compensation and

the centralized IMM, the actual motion of an object can be obtained and optimal solution can be provided. In addition, sensor failure cases among camera, RADAR, and LiDAR are considered to verify the robustness of the proposed object tracking performance against bad weather conditions. The proposed algorithms are verified based on the experimental data in several test scenarios. The main contributions of this paper can be summarized as follows:

- A novel formulation of IMM filter is proposed such that IMM filter is integrated with Centralized Kalman Filter (CKF) for enhanced multi-sensor data fusion.
- A track compensation algorithm in the moving reference frame is presented to track the actual motion of objects.
- A robust object tracking is pursued to address sensor failures due to various driving environment.
- The feasibility of the proposed algorithm is evaluated using experimental driving data.

II. RELATED WORKS

A. KF-BASED APPROACHES

For the state estimation, filtering techniques such as KF-based approaches have evolved to enhance estimation performance. Due to its ease of implementation and strong performance, the standard KF has been regarded as the most common filter. However, in automated driving environments, advanced versions of the KF are utilized because objects exhibit nonlinear behaviors and sensor measurements are uncertain. For instance, Extended Kalman Filter (EKF) [19] was applied to track nonlinear maneuvering objects, but it has limitations due to the linearization errors. As an improvement, the Unscented Kalman Filter (UKF) [20] was introduced, but it still requires further improvement of finding optimal parameters. The cubature KF, which enhances the convergence and estimation accuracy of the UKF, was proposed [21]. Efforts have been made to enhance the performance of the cubature KF by estimating an augmented state, which consists of state and process noise [22]. In addition to solutions for nonlinearity, there were several other studies for robust estimation, among which the H-infinity filter was developed to to minimize the worst-case estimation error within a specified bound [23]. In [24], the noise covariance adaption technique was applied to the H-infinity filter. However, the studies [19], [20], [21], [22], [23], [24] have limitations in that they use a single prediction model or are difficult to apply in multi-sensor environments.

B. IMM-BASED APPROACHES

Another approach for improving object tracking and estimation performance is the IMM-based filter, which has been increasingly employed recently [25]. This is due to the challenge in modeling the movements of various objects in the automated driving environment, as a single motion model may not be sufficient. For that reason, IMM, useful for estimating the state of objects whose class and maneuver are unknown, was first presented in [26]. However, the original IMM cannot handle models with different state dimensions and is influenced by the performance of the sub-filter, KF, indicating the need for further development. Subsequently, the IMM filter has evolved in various ways. Zubaca et al. [27] developed a novel mode mixing approach for IMM filters in vehicle motion models with unequal state dimensions, reducing the overall complexity and enhancing state estimation. Li and Bian [28] integrated IMM with a novel correlation filter for object tracking. Wenkang et al. [29] presented a vehicle state observer based on the IMM with a square root cubature KF. Lim et al. [30] proposed an IMM algorithm with a mini-max strategy for particle filtering. The studies [27], [28], [29], [30] improve the state estimation performance and implementation complexity of the original IMM filter in their own ways, but they still have the limitation of being difficult to utilize in multi-sensor environments.

C. FUSION STRUCTURES

Highly automated vehicles require robust perception capabilities for stable OEDR performance, and one of the methods to achieve the capability is the use of multiple sensors [31]. Consequently, research has been conducted to fuse multiple sensors, achieving superior object tracking performance compared to using a single sensor. Regarding the distributed fusion, reduced computational load on the central processing unit is the main advantage, whereas the solution is not theoretically optimal [32]. After Olfati-Saber proposed the Kalman Consensus Filter (KCF) [33] as a solution for distributed fusion, subsequent studies have been conducted to improve the performance of state estimation. For instance, the work in [34] introduced a distributed filtering algorithm, which breaks down the operations of optimal centralized Kalman filtering into manageable components for individual agents. Xin et al. [35] developed a trust-based classification fusion strategy for resisting sensor faults utilizing KCF. Yoon et al. [36] utilized multi-modal learning techniques to determine the weights for merging local tracks from multiple sensors.

Centralized structure can be adopted to reduce estimation errors for high-level fusion applications where data transmission can be managed with relatively limited bandwidth. Even though centralized fusion faces the practical issue of requiring substantial bandwidth to transmit raw data through the network, it offers the advantage of providing an optimal solution [2]. Cai et al. [37] utilized both centralized fusion incorporating multi-coordinate system for optimal estimation and distributed fusion using the covariance intersection method.

D. FUSION APPROACHES UTILIZING IMM

As reliable estimation performance is increasingly demanded in various applications, studies have been conducted to reduce estimation errors by utilizing multiple sensors [7]. Among the studies, efforts have been made to integrate the traditional IMM [26] into multi-sensor fusion systems. For instance, Hong-tao and Feng-ju [38] developed a measurement fusion algorithm that uses the least squares method to combine

multiple sensor measurements into a single measurement. This approach allows the IMM to function as in a single measurement environment. Cen et al. [39] and Zhifeng et al. [40] introduced multi-sensor IMM algorithms that use a global measurement vector, which concatenates all measured states into a single long vector. This vector allows the algorithm to update the state using the same formula as the single-sensor IMM.

However, a reconfiguration of the global measurement vector is required if any measurement becomes invalid, resulting in complexity and inconvenience. Cho et al. [41] and Yang et al. [42] introduced a distributed IMM structure in which each sensor has its own IMM filter, consisting of several sub-filters and a main filter. However, this approach poses challenges in adjusting each filter's parameters and does not provide the true optimal solution in sensor fusion. Furthermore, as the number of sensors increases, the total amount of the required calculation significantly increases.

Centralized fusion algorithms for multi-sensor system with bounded disturbances were presented based on ellipsoidal bounding estimation [43]. Fatih Kara and Başaran [44] developed an IMM for train position estimation and integrated it with a KCF using weighted averages to fuse heterogeneous sensor data. Qiu et al. [45] integrated the IMM approach with an adaptive CKF for underwater object tracking. Wang and Li [46] presented an integration of the federated filtering with the adaptive IMM for global positioning. Yang and Zuo [47] exploited the distributed structure based on simple convex covariance for sensor fusion and applied it to the IMM.

E. MOVING REFERENCE FRAME

When using the IMM for object tracking in a moving reference frame, there are certain situations where the motion of objects is not properly estimated. For example, consider a situation where both the host and surrounding vehicles travel in a lane with constant curvature at the same speed. In this situation, the IMM may perceive the surrounding vehicle as stationary due to unvarying measurement. Although setting states and measurements as absolute values can partially resolve the situation, the problem of unreliable tracking results due to unstable GPS signals still remains. To address the problem, Altendorfer [48] proposed a mixed coordinate system. Farrell [49] researched the integration of the Coriolis force, centripetal force, and gravitational force, each of which can influence the flight trajectory of a ballistic missile, into their motion models. This research was done to enable the IMM to conduct precise missile tracking. Chen et al. [50] resolved the track-to-track association issue caused by sensor biases by employing polar coordinates. Jo et al. [51] resolved the issue by transforming the state and measurement into curvilinear coordinates.

The rest of this paper is organized as follows. In Section III, the CKF and its adaptation to the IMM filter are introduced in detail. In Section IV, the track compensation algorithm is explained using the case of lane changing as an example. In Section V, the performance of the proposed algorithm is evaluated using real-vehicle experimental data obtained in several test scenarios.

III. CENTRALIZED IMM FILTER FOR THE MULTI-MEASUREMENT ENVIRONMENT

This section presents a novel formulation of the IMM filter for multi-measurement systems as illustrated in Fig 2. In Section III-A, a system model for tracking nonlinear maneuvering objects is presented, and the system model variables and motion models used in the IMM filter are discussed. For the centralized sensor fusion approach, CKF are briefly summarized in Section III-B. In Section III-C, the proposed integration of the centralized IMM filter with the CKF is explained, along with the differences from the existing methods.

A. PRELIMINARIES

A nonlinear maneuvering object tracking system with additive noise and its linear sensing model can be described as

$$\begin{aligned} x_k &= f\left(x_{k-1}\right) + \Gamma\omega_k \\ z_{j,k} &= H_{j,k}x_k + \upsilon_{j,k} \end{aligned} \tag{1}$$

x_k represents the state vector at the time instance k as

$$x_k = \begin{bmatrix} x_{\text{pos},k} & y_{\text{pos},k} & v_k & \psi_k & \dot{\psi}_k \end{bmatrix}^T \tag{2}$$

where

$x_{\text{pos},k}$: relative longitudinal distance
$y_{\text{pos},k}$: relative lateral distance
v_k : absolute speed
ψ_k : relative yaw angle
$\dot{\psi}_k$: absolute yaw rate

Note that x_k is defined in a hybrid coordinate system for the track compensation algorithm in Section IV where $x_{\text{pos},k}$, $y_{\text{pos},k}$, and ψ_k are set as relative values, and v_k and $\dot{\psi}_k$ are set as absolute values. The description of the state is illustrated in Fig. 3. The operator $f(\cdot)$ represents the nonlinear maneuver of an object and can be expressed as (8), (9), and (10). $\omega_k \sim \mathcal{N}(0, Q)$ is the process noise which is assumed to be zero-mean Gaussian distributed with covariance, Q, and Γ is the associated noise input matrix.

$$\begin{aligned} Q &= \begin{bmatrix} \sigma_v^2 & 0 \\ 0 & \sigma_{\dot{\psi}}^2 \end{bmatrix} \\ \Gamma &= \begin{bmatrix} 0 & 0 & 1 & 0 & 0 \\ 0 & 0 & 0 & 0 & 1 \end{bmatrix}^T \end{aligned} \tag{3}$$

σ_v and $\sigma_{\dot{\psi}}$ denote standard deviation of predicted speed and yaw rate, respectively, and they are tuning parameters that affect the estimation performance. According to [12] and [52], discrete time process noise covariance, Q_k, is obtained as

$$Q_k = \int_0^{\Delta t} e^{\nabla f \tau} \Gamma Q \Gamma^T \left(e^{\nabla f \tau}\right)^T d\tau \tag{4}$$

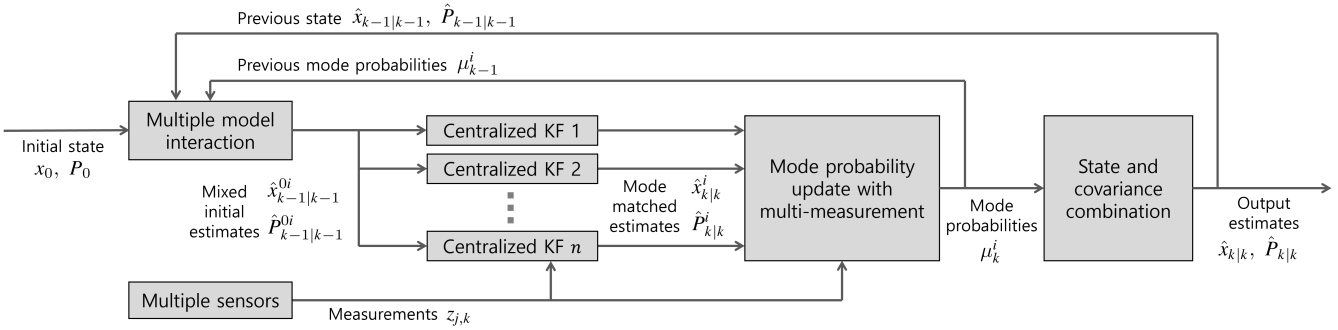

FIGURE 2. Overall architecture of the proposed IMM filter.

where

Δt: sampling time
∇f: jacobian matrix of $f(\cdot)$

$z_{j,k}$ is the observation acquired by sensors. In this study, four environmental sensors are utilized for object tracking and they are commercial camera, RADAR, and two LiDARs. Observation set, Z_k, is assumed to be synchronous to time instance k, and also assumed to be associated with a track.

$$Z_k = \{z_{j,k} \mid j = \text{Camera},\ \text{RADAR},\ \text{LiDAR}_1,\ \text{LiDAR}_2\} \tag{5}$$

Each sensor measurement vector, $z_{j,k}$, is defined as

$$\begin{aligned} z_{\text{Camera},k} &= \begin{bmatrix} x_{\text{pos},k} & y_{\text{pos},k} \end{bmatrix}^T \\ z_{\text{RADAR},k} &= \begin{bmatrix} x_{\text{pos},k} & y_{\text{pos},k} & v_{\text{sensor},k} + v_{\text{host},k} \end{bmatrix}^T \\ z_{\text{LiDAR}_1,k} &= \begin{bmatrix} x_{\text{pos},k} & y_{\text{pos},k} & v_{\text{sensor},k} + v_{\text{host},k} & \psi_k \end{bmatrix}^T \\ z_{\text{LiDAR}_2,k} &= \begin{bmatrix} x_{\text{pos},k} & y_{\text{pos},k} & v_{\text{sensor},k} + v_{\text{host},k} & \psi_k \end{bmatrix}^T \end{aligned} \tag{6}$$

where $v_{\text{sensor},k}$ and $v_{\text{host},k}$ denote the relative speed of an object from environmental sensors and the speed of the Host Vehicle (HV) from an in-vehicle sensor, respectively. Since the speed of the state has absolute values, the HV's speed, $v_{\text{host},k}$, is added to the sensor's speed measurement, $v_{\text{sensor},k}$. The observation matrix, $H_{j,k}$, should be suitably set according to dimension of the vector $z_{j,k}$. For instance, $H_{\text{Camera},k}$ is set as follows:

$$H_{\text{Camera},k} = \begin{bmatrix} 1 & 0 & 0 & 0 & 0 \\ 0 & 1 & 0 & 0 & 0 \end{bmatrix} \tag{7}$$

$\upsilon_{j,k} \sim \mathcal{N}(0, R_{j,k})$ represents the vector-valued observation noise which is assumed to be zero-mean Gaussian distributed with covariance $R_{j,k}$. There are several methods to determine the covariance, $R_{j,k}$, including referencing the sensor's specifications, making heuristic determination [53], or obtaining it through adaptive covariance matrix calculations [54].

IMM-based object tracking algorithms employ the several motion models. Three motion models are commonly used in IMM-based approaches: static motion model [55], Constant Velocity (CV) model [56], and Constant Turn Rate and Velocity (CTRV) model [57]. The static motion model is applied to track stationary objects and randomly moving objects such as pedestrians or objects with noisy measurements [55]. The yaw rate is fixed to zero, and all other states remain unchanged from the previous states for the operator, $f(\cdot)$, in (1)

$$f^{\text{Static}}(x_k) = \begin{bmatrix} x_{\text{pos},k} & y_{\text{pos},k} & v_k & \psi_k & 0 \end{bmatrix}^T \tag{8}$$

The CV model predicts that the object will proceed along a straight, unchanging route with respect to speed and direction. It shows good performance when tracking the lane keeping vehicles at high speeds [56].

$$\begin{aligned} &f^{\text{CV}}(x_k) \\ &= \begin{bmatrix} x_{\text{pos},k} + \Delta t \cdot v_k \cdot \cos\psi_k & y_{\text{pos},k} + \Delta t \cdot v_k \cdot \sin\psi_k \\ v_k & \psi_k & 0 \end{bmatrix}^T \end{aligned} \tag{9}$$

The CTRV model is used for tracking objects that are moving in a circular path with a constant turning radius. The model assumes that the yaw rate is fixed at a specific value,

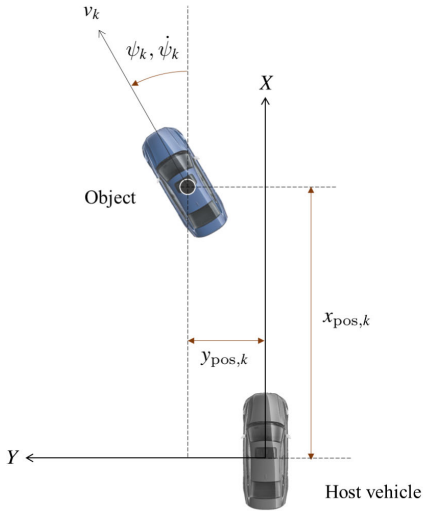

FIGURE 3. Definition of the object's state.

and it is equivalent to incorporating rotational motion into the CV model [57].

$$f^{\text{CTRV}}(x_k) = \Bigg[x_{\text{pos},k} + \frac{v_k}{\dot{\psi}_k}\left(\sin\left(\psi_k + \Delta t \cdot \dot{\psi}_k\right) - \sin\psi_k\right) \quad y_{\text{pos},k} + \frac{v_k}{\dot{\psi}_k}\left(\cos\psi_k - \cos\left(\psi_k + \Delta t \cdot \dot{\psi}_k\right)\right) \quad v_k \quad \psi_k + \Delta t \cdot \dot{\psi}_k \quad \dot{\psi}_k \Bigg]^T \tag{10}$$

The nonlinear state transition functions of CV and CTRV models are linearized for use in the prediction step of the CKF. As in [12], (11) is obtained following the linearized discretization approach under zero-order hold assumption.

$$F_k^{\text{Static}} = \left.\frac{\partial f^{\text{Static}}}{\partial x}\right|_{x_k}$$
$$F_k^{\text{CV}} = \left.\frac{\partial f^{\text{CV}}}{\partial x}\right|_{x_k}$$
$$F_k^{\text{CTRV}} = \left.\frac{\partial f^{\text{CTRV}}}{\partial x}\right|_{x_k} \tag{11}$$

B. SUMMARY OF THE CENTRALIZED KALMAN FILTER

Since environmental sensors such as RADAR, LiDAR, and cameras have their own sensing characteristics, the measurement noise covariance corresponding to each sensor has different values. To avoid sub-optimal results, the WLS method [11] can be utilized, which provides optimal estimates over heterogeneous measurements. After the WLS estimates and its covariance of the given sensing model in (1) are computed by using the IF form [12], the WLS estimates can be transformed into the following alternative sequential information form [13], [58].

$$\hat{P}_{k|k} = \left[P_{k|k-1}^{-1} + \sum_{j=1}^{N_s} H_{j,k}^T R_{j,k}^{-1} H_{j,k} \right]^{-1}$$
$$\hat{x}_{k|k} = \hat{P}_{k|k}\left[P_{k|k-1}^{-1} x_{k|k-1} + \sum_{j=1}^{N_s} H_{j,k}^T R_{j,k}^{-1} z_{j,k} \right] \tag{12}$$

where

$\hat{x}_{k\|k}$:	updated state estimates
$\hat{P}_{k\|k}$:	updated covariance estimates
$x_{k\|k-1}$:	predicted state
$P_{k\|k-1}$:	predicted covariance
N_s:	number of observations associated with a track

Because the full past observations are not required to estimate the state, (12) has computational efficiency similar to the original KF.

C. CENTRALIZED IMM FILTER DESIGN

Equation (12) can be applied to the state estimation process of the IMM filter [59] as illustrated in Fig. 2, allowing for a new IMM to be derived. First, it is necessary to update the mode probability using the multi-measurement system. For a multi-measurement system, the probability of the i-th mode at time step k can be derived as:

$$\begin{aligned}
\mu_k^i &= p\left(i|z_{j,0:k}\right) \\
&\propto p\left(z_{1,k}, z_{2,k}, \ldots, z_{N_s,k}|z_{j,0:k-1}, i\right) \cdot p\left(i|z_{j,0:k-1}\right) \\
&= p\left(z_{1,k}|z_{j,0:k-1}, i\right) \cdot p\left(z_{2,k}|z_{j,0:k-1}, i\right) \cdot \cdots \\
&\quad \cdot p\left(z_{N_s,k}|z_{j,0:k-1}, i\right) \cdot p\left(i|z_{j,0:k-1}\right) \\
&= \mathcal{N}\left(z_{1,k}; z_{j,k|k-1}^i, S_{1,k}^i\right) \cdot \mathcal{N}\left(z_{2,k}; z_{j,k|k-1}^i, S_{2,k}^i\right) \cdot \cdots \\
&\quad \cdot \mathcal{N}\left(z_{N_s,k}; z_{j,k|k-1}^i, S_{N_s,k}^i\right) \cdot \sum_{m=1}^{N_m} \pi_{mi}\mu_{k-1}^m \\
&= \prod_{j=1}^{N_s} \mathcal{N}\left(z_{j,k}; z_{j,k|k-1}^i, S_{j,k}^i\right) \cdot \sum_{m=1}^{N_m} \pi_{mi}\mu_{k-1}^m
\end{aligned} \tag{13}$$

where

i :	mode state with $i \in \{1, 2, \ldots, N_m\}$
j :	measurement index with $j \in \{1, 2, \ldots, N_s\}$
μ_k^i :	mode probability of the i-th mode
$z_{0:k}$:	measurements of all sensors from the time 0 to k
$z_{j,k}^i$:	transformed predicted state of i-th mode to j-th measurement space
$S_{j,k}^i$:	variance of the measurement $z_{j,k}$
π_{mi}:	probability of transition from mode m to i
N_m :	number of motion models
$\mathcal{N}(\cdot)$:	probability density function of the Gaussian distribution
$p\left(z_{j,k}\|z_{j,0:k-1}, i\right)$:	conditional probability of obtaining j-th measurement at time k, given j-th measurements up to time $k-1$ and the mode is i at time k

In (13), $p\left(z_{1,k}, z_{2,k}, \ldots, z_{N_s,k}|z_{j,0:k-1}, i\right)$ is divided into terms corresponding to each sensor because observation events from each sensor data can be considered independent. In other words, by multiplying the observation probabilities of the sensors, multi-sensor fusion can be applied to the IMM filter. As a result, normalized posterior mode probabilities are calculated as

$$\mu_k^i = \frac{\prod_{j=1}^{N_s} \mathcal{N}\left(z_{j,k}; z_{j,k|k-1}^i, S_{j,k}^i\right) \cdot \sum_{m=1}^{N_m} \pi_{mi}\mu_{k-1}^m}{\sum_{n=1}^{N_m}\left(\prod_{j=1}^{N_s} \mathcal{N}\left(z_{j,k}; z_{j,k|k-1}^n, S_{j,k}^n\right) \cdot \sum_{m=1}^{N_m} \pi_{mi}\mu_{k-1}^n\right)} \tag{14}$$

Consequently, using (14), the process of the multi-measurement IMM can be summarized as follows:

1) MULTIPLE MODEL INTERACTION

- Mixing probabilities
  In the IMM filter, the states from the previous step of each model are integrated using the mixing probability [60]. $\mu^{mi}_{k-1|k-1}$ represents the probability that mode m was active at time step $k-1$, given that mode i is active at time step k. The probability can be regarded as the normalized weight of each mode to the mixed state and covariance.

$$\mu^{mi}_{k-1|k-1} = \frac{\pi_{mi}\mu^{m}_{k-1}}{\sum_{l=1}^{N_m}\pi_{li}\mu^{l}_{k-1}} \tag{15}$$

  where π_{mi} represents the probability that the mode which was m at $k-1$ transitions to i at k. The transition probability matrix, π, which represents the probability of mode changes, is chosen empirically for the best estimation performance.

$$\pi = \begin{bmatrix} 0.995 & 0.0025 & 0.0025 \\ 0.0025 & 0.995 & 0.0025 \\ 0.0025 & 0.0025 & 0.995 \end{bmatrix}$$

- Mixed states and covariance
  The interaction among the models is utilized to obtain the mixed initial state and its covariance by using (15). Equation (16) determines the initial state, $\hat{x}^{0i}_{k-1|k-1}$, and the initial covariance, $\hat{P}^{0i}_{k-1|k-1}$, for mode i at time step k by weighted summation of the state and covariance estimates of each mode at time step $k-1$. Initial state and covariance are then provided as inputs to the sub-filters of the IMM corresponding to each motion model.

$$\begin{aligned}\hat{x}^{0i}_{k-1|k-1} &= \sum_{m=1}^{N_m}\mu^{mi}_{k-1|k-1}\hat{x}^{m}_{k-1|k-1} \\ \hat{P}^{0i}_{k-1|k-1} &= \sum_{m=1}^{N_m}\mu^{mi}_{k-1|k-1} \\ &\quad\left[\hat{P}^{m}_{k-1|k-1} + \left(\hat{x}^{m}_{k-1|k-1} - \hat{x}^{0i}_{k-1|k-1}\right)\right. \\ &\quad\left.\cdot\left(\hat{x}^{m}_{k-1|k-1} - \hat{x}^{0i}_{k-1|k-1}\right)^{T}\right]\end{aligned} \tag{16}$$

  where $\hat{x}^{m}_{k-1|k-1}$ and $\hat{P}^{m}_{k-1|k-1}$ denote the previous state estimates of m-th mode and its covariance, respectively.

2) MODE-MATCHED STATE ESTIMATION

- Prediction
  In the prediction step, each sub-filters propagate its initial state and covariance forward in time. The state transition matrix, F^{i}_{k}, of i-th mode is the Jacobian matrix of i-th nonlinear state as shown in (11). The process noise matrix, Q^{i}_{k}, of i-th mode is sampled from (4).

$$\begin{aligned}x^{i}_{k|k-1} &= F^{i}_{k}\hat{x}^{0i}_{k-1|k-1} \\ P^{i}_{k|k-1} &= F^{i}_{k}\hat{P}^{0i}_{k-1|k-1}\left(F^{i}_{k}\right)^{T} + Q^{i}_{k}\end{aligned} \tag{17}$$

- Measurement update
  Each sub-filter calculates the updated state estimate, $\hat{x}^{i}_{k|k}$, and its covariance, $\hat{P}^{i}_{k|k}$, utilizing the CKF in Section III-B.

$$\begin{aligned}\hat{P}^{i}_{k|k} &= \left[\left(P^{i}_{k|k-1}\right)^{-1} + \sum_{j=1}^{N_s}H^{T}_{j,k}R^{-1}_{j,k}H^{i}_{j,k}\right]^{-1} \\ \hat{x}^{i}_{k|k} &= \hat{P}^{i}_{k|k}\left[\left(P^{i}_{k|k-1}\right)^{-1}x^{i}_{k|k-1} + \sum_{j=1}^{N_s}H^{T}_{j,k}R^{-1}_{j,k}z_{j,k}\right]\end{aligned} \tag{18}$$

3) MODE PROBABILITY UPDATE

- The covariance, $S^{i}_{j,k}$, for the residual of the observation is calculated from the output of each sub-filter. Then, the i-th mode probability, μ^{i}_{k}, corresponding to i-th motion model is calculated using (14) with

$$\begin{aligned}z^{i}_{j,k|k-1} &= H_{j,k}x^{i}_{k|k-1} \\ S^{i}_{j,k} &= H_{j,k}P^{i}_{k|k-1}H^{T}_{j,k} + R_{j,k}\end{aligned} \tag{19}$$

4) OUTPUT STATE AND COVARIANCE

- The mode probability μ^{i}_{k} represents the contribution of each mode to the combined output state and covariance. Then, using the Gaussian mixture [9], state estimates, $\hat{x}_{k|k}$, and covariance estimates, $\hat{P}_{k|k}$, can be calculated.

$$\begin{aligned}\hat{x}_{k|k} &= \sum_{i=1}^{N_m}\mu^{i}_{k}\hat{x}^{i}_{k|k} \\ \hat{P}_{k|k} &= \sum_{i=1}^{N_m}\mu^{i}_{k}\left[\hat{P}^{i}_{k|k} + \left(\hat{x}^{i}_{k|k} - \hat{x}_{k|k}\right)\left(\hat{x}^{i}_{k|k} - \hat{x}_{k|k}\right)^{T}\right]\end{aligned} \tag{20}$$

IV. TRACK COMPENSATION FOR THE IMM FILTER

A. BACKGROUND

In a moving reference frame using an IMM filter for object tracking, unintended results can be obtained as explained in Section II-E. If both vehicles maintain the same speed, onboard sensor measurements will indicate no change in the position, speed, or heading angle of the surrounding vehicle as shown in Fig. 4. In this study, a track compensation algorithm is proposed to determine the actual motion of objects, which is neither dependent on localization performance nor affected by GPS failure. Since the proposed algorithm exclusively utilizes information from in-vehicle sensors such as the wheel speed sensor and the yaw rate sensor, it remains unaffected by the antenna status or the localization results.

B. COMPENSATION ALGORITHM DESIGN

The proposed compensation algorithm operates just before the IMM filtering process for object (track) state estimation

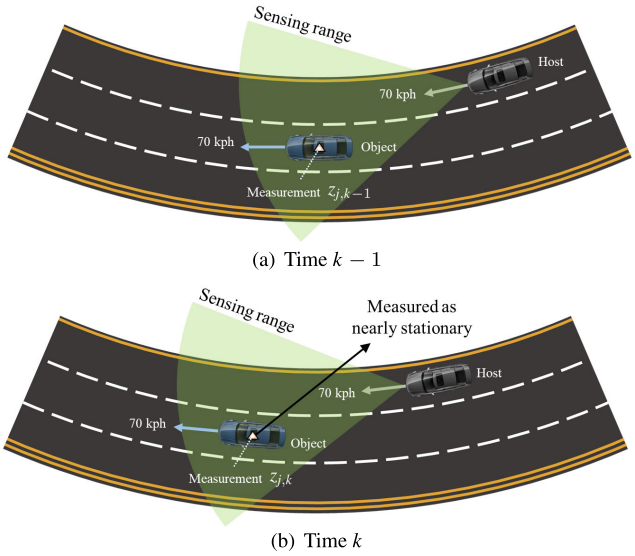

FIGURE 4. A case of stationary measurement in the moving reference frame.

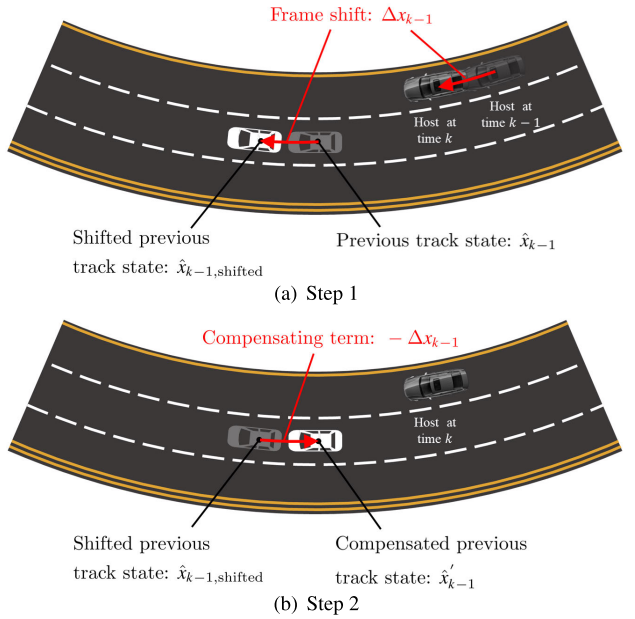

FIGURE 5. Sequence of the track compensation.

at time k. The algorithm has two steps, where the first step calculates the change in the HV's state, Δx_{k-1}, during the time from $k-1$ to k.

$$\begin{aligned}\Delta x_{k-1} &= f\left(v_{\text{host},k-1},\ \dot{\psi}_{\text{host},k-1},\ \Delta t\right)\\ &= \begin{bmatrix} \frac{v_{\text{host},k-1}}{\dot{\psi}_{\text{host},k-1}} \sin\left(\Delta t \cdot \dot{\psi}_{\text{host},k-1}\right) \\ \frac{v_{\text{host},k-1}}{\dot{\psi}_{\text{host},k-1}} \left(1-\cos\left(\Delta t \cdot \dot{\psi}_{\text{host},k-1}\right)\right) \\ 0 \\ \Delta t \cdot \dot{\psi}_{\text{host},k-1} \\ 0 \end{bmatrix}\end{aligned} \tag{21}$$

where Δt represents the time interval from $k-1$ to k. The change in the state of the HV, Δx_{k-1}, is calculated under the

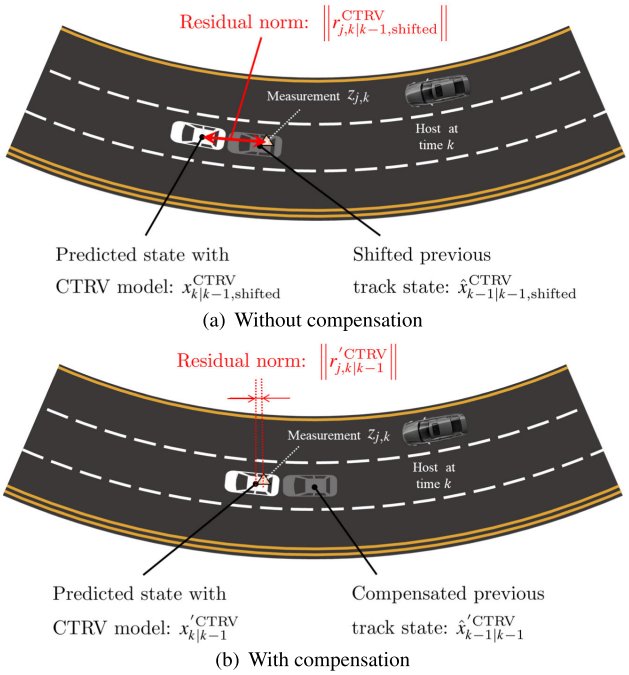

FIGURE 6. Residual comparison for CTRV model.

assumption that its speed, $v_{\text{host},k-1}$, and yaw rate, $\dot{\psi}_{\text{host},k-1}$, remain constant during Δt. The first step of the algorithm calculates how much the reference frame shifted. As the frame shifted, so does the previous track state, $\hat{x}_{k-1}$, which shifts into $\hat{x}_{k-1,\text{shifted}}$ as illustrated in Fig. 5(a). Because the values allocated in the processing unit's memory remain unchanged, $\hat{x}_{k-1}$ and $\hat{x}_{k-1,\text{shifted}}$ have the same numerical values.

$$\hat{x}_{k-1,\text{shifted}} = \hat{x}_{k-1} \tag{22}$$

However, due to the shift in the reference frame, they exhibit a difference of Δx_{k-1} in a physical sense. In the second step, the compensated previous track state, $\hat{x}'_{k-1}$, is obtained by subtracting the physical difference, Δx_{k-1}, from the shifted track, $\hat{x}_{k-1,\text{shifted}}$, as illustrated in Fig. 5(b).

$$\hat{x}'_{k-1} = \hat{x}_{k-1,\text{shifted}} - \Delta x_{k-1} \tag{23}$$

By compensating $\hat{x}_{k-1,\text{shifted}}$ with $-\Delta x_{k-1}$, true previous state estimates, $\hat{x}'_{k-1}$, in the reference frame at time k can be obtained. The compensation algorithm computes $\hat{x}'_{k-1}$ before the IMM filter operates at time k. Subsequently, $\hat{x}'_{k-1}$ is used in (16) to calculate the initial state, $\hat{x}^{0i}_{k-1|k-1}$, and initial covariance, $\hat{P}^{0i}_{k-1|k-1}$. Therefore, the compensating process is repeated for the number of modes, N_m, defined in the IMM, and (16) and (23) can be rewritten as

$$\hat{x}^{0i}_{k-1|k-1} = \sum_{m=1}^{N_m} \mu^{mi}_{k-1|k-1} \hat{x}'^{m}_{k-1|k-1}$$

$$\hat{P}^{0i}_{k-1|k-1} = \sum_{m=1}^{N_m} \mu^{mi}_{k-1|k-1}$$

$$\times \left[\hat{P}^{m}_{k-1|k-1} + \left(\hat{x}^{'m}_{k-1|k-1} - \hat{x}^{0i}_{k-1|k-1} \right) \cdot \left(\hat{x}^{'m}_{k-1|k-1} - \hat{x}^{0i}_{k-1|k-1} \right)^{T} \right] \tag{24}$$

where

$$\hat{x}^{'m}_{k-1|k-1} = \hat{x}^{m}_{k-1|k-1,\text{shifted}} - \Delta x_{k-1}$$
$$i = 1, 2, \ldots, N_m$$

In the perspective of filtering, the proposed compensation algorithm induces an error of Δx_{k-1} in the state estimate. This error affects the residuals between the state predictions and the sensor measurements. Equation (25) demonstrates that the residual with the compensation is smaller than the residual without the compensation as illustrated in Fig. 6.

$$\left\| r^{'\text{CTRV}}_{j,k|k-1} \right\| < \left\| r^{\text{CTRV}}_{j,k|k-1,\text{shifted}} \right\|, \quad j = 1, 2, \ldots, N_s \tag{25}$$

where

$$r^{'\text{CTRV}}_{j,k|k-1} = z_{j,k} - H_{j,k} x^{'\text{CTRV}}_{k|k-1}$$
$$r^{\text{CTRV}}_{j,k|k-1,\text{shifted}} = z_{j,k} - H_{j,k} x^{\text{CTRV}}_{k|k-1,\text{shifted}}$$

Referring to (13), the smaller the magnitude of the residual, the higher the mode probability the IMM filter assigns to that mode.

$$\mu^{i}_{k} \propto \mathcal{N}\left(z_{j,k}; z^{i}_{j,k|k-1}, S^{i}_{j,k} \right) = \frac{1}{\sqrt{2\pi \left| S^{i}_{j,k} \right|}} \exp\left(- \frac{r^{i}_{j,k|k-1}{}^{T} S^{i}_{j,k}{}^{-1} r^{i}_{j,k|k-1}}{2} \right) \tag{26}$$

where

$$r^{i}_{j,k|k-1} = z_{j,k} - H_{j,k} x^{i}_{k|k-1}$$

Therefore, it can be inferred that the compensation algorithm, which enables obtaining a higher probability, estimates the actual motion of the object better. Fig. 7 compares the residuals for each mode where green, blue and red colored lines represent static, CV and CTRV models, respectively. As illustrated in Fig. 7(a), the magnitude of the static model's mode residual is smaller compared to those of other modes when the state is not compensated. Hence, as expressed in (27), the mode probability of the static model, μ^{Static}_{k}, is greater than that of the CTRV, μ^{CTRV}_{k}. Since the object is actually in constant turning motion, this result is incorrect, as discussed in Section IV-A.

$$\mu^{\text{CTRV}}_{k} < \mu^{\text{Static}}_{k} \tag{27}$$

where

$$\left\| r^{\text{CTRV}}_{j,k|k-1,\text{shifted}} \right\| > \left\| r^{\text{Static}}_{j,k|k-1,\text{shifted}} \right\|$$

Conversely, when the state is compensated, the magnitude of the CTRV's mode residual is smaller than that of the static model, indicating that the CTRV model is assigned a higher probability, as shown in (28) and Fig. 7(b).

$$\mu^{\text{CTRV}}_{k} > \mu^{\text{Static}}_{k} \tag{28}$$

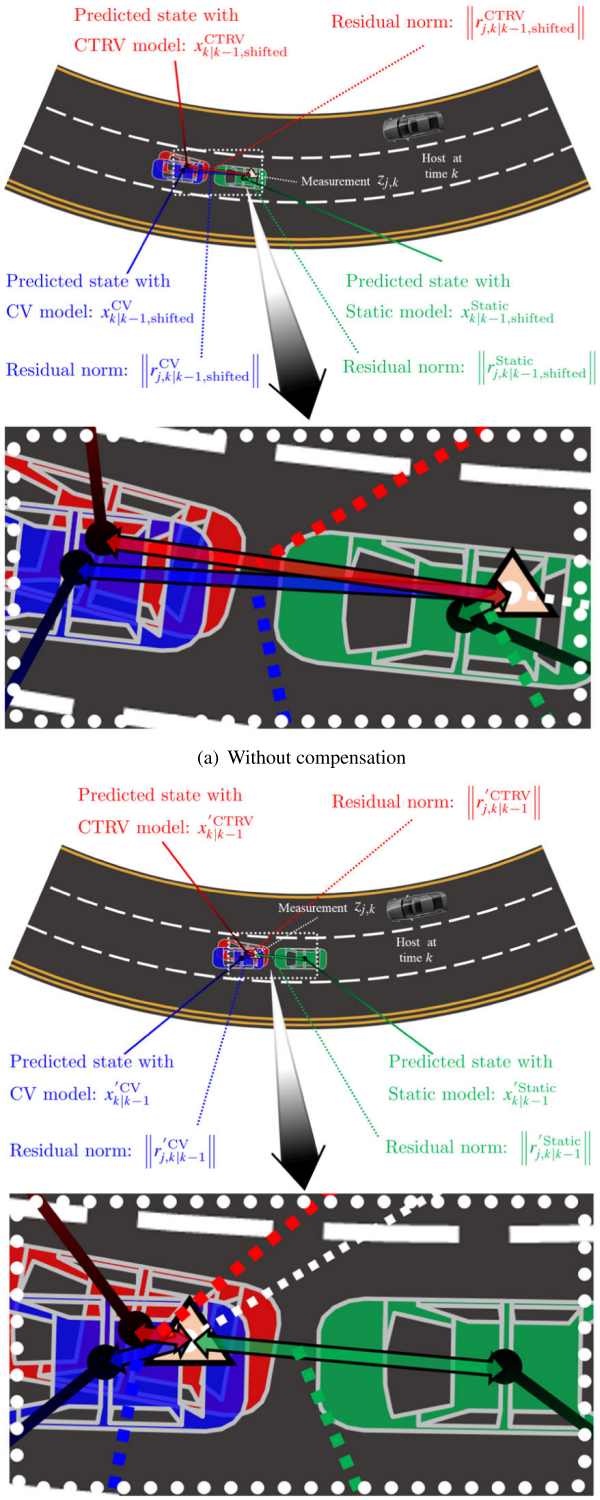

FIGURE 7. Residual comparison for all models.

where

$$\left\| r^{'\text{CTRV}}_{j,k|k-1} \right\| < \left\| r^{'\text{Static}}_{j,k|k-1} \right\|$$

Through the case study in figures 4 through 7, it is demonstrated that the proposed track compensation algorithm

resolves issues arising in object tracking within a moving reference frame. With the compensation, accurate estimation of the object's actual motion is possible even without localization. Therefore, object tracking functionality is maintained even in the failure case of a global positioning sensor.

V. EXPERIMENTAL RESULTS

Experiments were conducted to detect the forward objects through camera sensor, RADAR and two LiDARs. A commercial camera providing object's position and a RADAR providing object's position and speed are installed on the vehicle. One of LiDARs is a commercial solid-state LiDAR, and the other is 360-degree 3D spinning LiDAR, and they are denoted as LiDAR 1 and LiDAR 2, respectively. A V2V (Vehicle-to-Vehicle) data transceiver is additionally installed to verify the performance of the proposed algorithm. The transmitter of the Target Vehicle (TV) equipped with GPS sends V2V data to the receiver of the HV. This data consists of global position and speed of the TV. Based on the GPS data of the HV and V2V information, the local position of the TV is calculated and considered as the ground truth. In this study, the state of the track from the proposed algorithm is compared to the ground truth. The complete sensor setup is shown in Fig. 8.

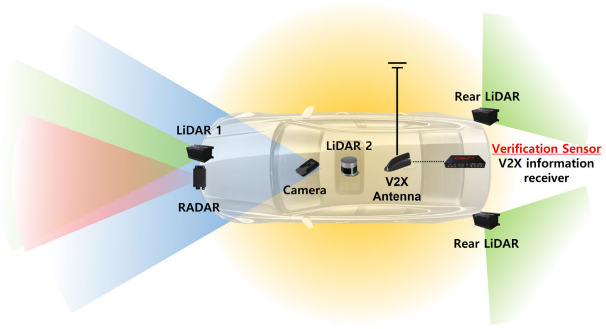

FIGURE 8. Sensor configuration.

A. EVALUATION OF THE CENTRALIZED SENSOR FUSION SYSTEM

In this section, the proposed sensor fusion algorithm, IMM-CKF, is compared with two methods: IMM-DKF [42] and CA-CKF. The IMM-DKF, which applies the Distributed KF instead of the CKF to the IMM filter, is chosen to compare the centralized and distributed structures. The CA-CKF, which integrates the Constant Acceleration (CA) model instead of the IMM, is selected to evaluate the tracking performance and the track compensation algorithm.

Three maneuvering scenarios were tested as shown in Fig. 9 where all sensors were normal. For the first scenario, the TV on the next lane attempts cut-in while the HV is driving at constant speed. In the second scenario, the HV changes a lane while the TV maintains a constant speed. Finally, in the third scenario, the TV performs multiple lane changes in front of the HV. The tracking results are illustrated in Fig. 10, 11, and 12, which show measurements from sensors, the trajectory of the object, and the sensor fusion results.

Figs. 10 through 12 show that the IMM-CKF produces superior results compared to the measurement of individual sensor. Even if there exist sensing errors in sensor measurements, the proposed method provides smoother and more accurate results than any individual sensor output. In addition, subplots in Fig. 10 through 12 demonstrate that the CA-CKF generates larger estimation errors compared to the IMM-CKF. This is because the prediction uncertainty of the single model increases when the actual motion of the object is different from the motion model output. Therefore, the use of multiple motion models for the state estimation, as in the proposed method, is necessary to improve the accuracy of the estimation results.

With the distributed sensor fusion structure such as IMM-DKF, errors or biases in specific sensor measurements can lead to performance degradation because the result is determined by the weighted sum of its filter estimates. On the other hand, the centralized filter integrates sensor data at once during the measurement update step. In this step, the weight between the predicted state and measurements can be adjusted. By increasing the weight of reliable sensors or predicted states instead of noisy measurements, it is possible to calculate the estimates to achieve robust tracking. As illustrated in the subplots of Figs. 10 through 12, despite large sensing errors in RADAR, LiDARs and/or camera sensors, IMM-CKF provides the object trajectory that closely matches with the ground truth. This indicates that even in the presence of measurement errors, consistent results can be still achieved by incorporating information from the other sensors. The accuracy results of the proposed method are compared in Table. 1 where the Average Root Mean Square Error (ARMSE) is used as a measure of the position accuracy. The results show that the proposed method outperforms each sensor output and other sensor fusion methods.

$$\text{ARMSE} = \sqrt{\frac{1}{n}\sum_{k=1}^{n}\left(q_k^* - \hat{q}_k\right)^T\left(q_k^* - \hat{q}_k\right)} \tag{29}$$

where

n : sum of time steps of each scenario

$q_k^* = \begin{bmatrix} 1 & 0 & 0 & 0 & 0 \\ 0 & 1 & 0 & 0 & 0 \end{bmatrix} x_k^*$

$\hat{q}_k = \begin{bmatrix} 1 & 0 & 0 & 0 & 0 \\ 0 & 1 & 0 & 0 & 0 \end{bmatrix} \hat{x}_{k|k}$

x_k^* : ground truth at time k

$\hat{x}_{k|k}$: state estimates at time k

For a comprehensive performance evaluation of the proposed method, the Cumulative Distribution Function (CDF) [61] is utilized as a metric. The Euclidean Distance Error (EDE) is used as the variable of the CDF, and the distance error at time step k is denoted as EDE_k, which is defined

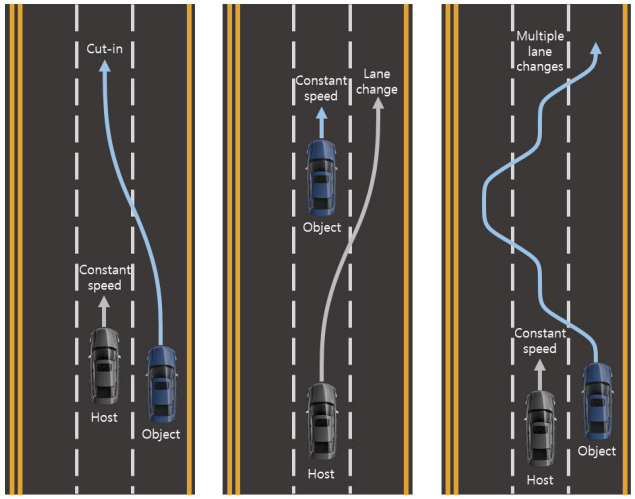

FIGURE 9. Test scenarios for object tracking.

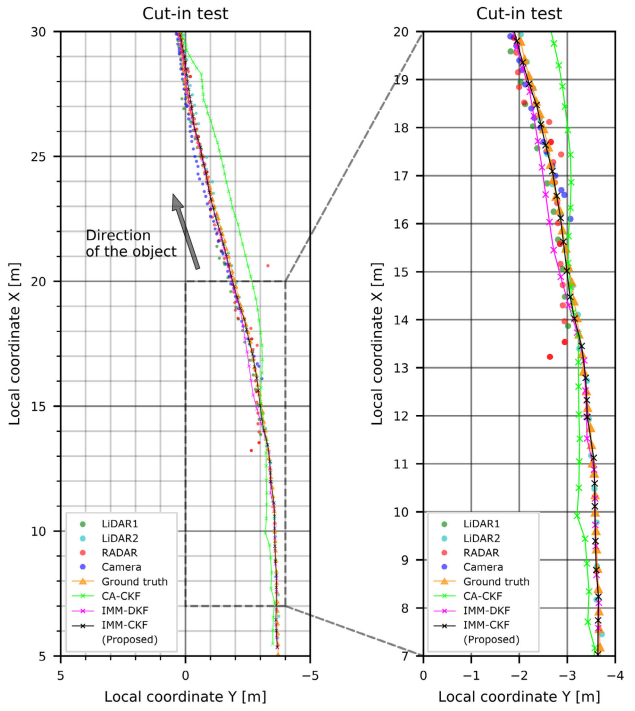

FIGURE 10. Tracking results of scenario 1.

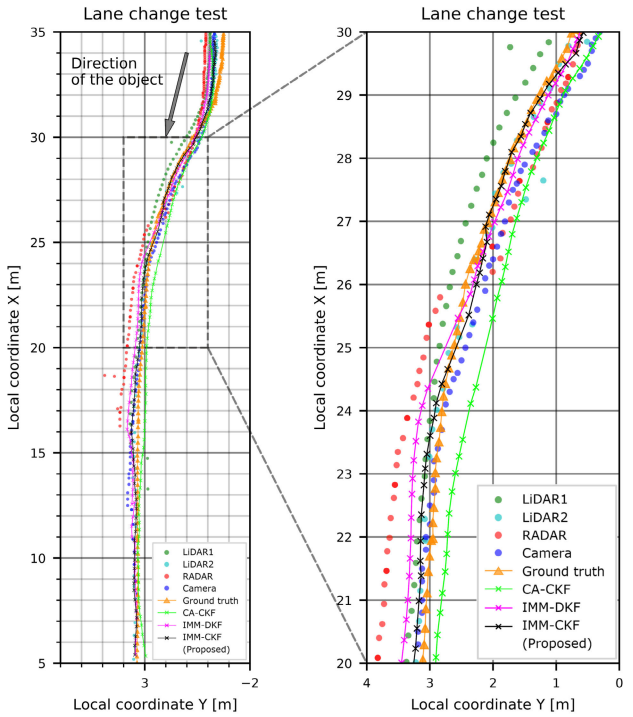

FIGURE 11. Tracking results of scenario 2.

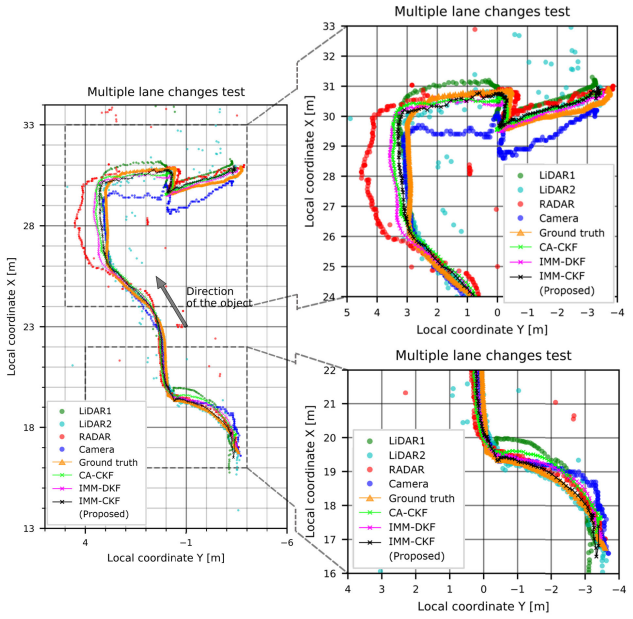

FIGURE 12. Tracking results of scenario 3.

by (30). EDE_k is calculated and stacked for the reference algorithms and sensor data during experiments. The set of stacked errors, EDEs, is expressed by (30) and is sorted in ascending order after the experiments. The sorted EDEs are denoted as EDEs*. The indices corresponding to each element of EDEs* are normalized by the size of the EDEs set, and their collection is defined as CDF*.

$$\mathrm{EDE}_k = \sqrt{\left(q_k^* - \hat{q}_k\right)^T \left(q_k^* - \hat{q}_k\right)}$$
$$\mathrm{EDEs} = \{\mathrm{EDE}_k | k \in \{1, 2, \ldots, n\}\}$$

$$\mathrm{EDEs}^* = \left\{\mathrm{EDE}_{k_1}, \mathrm{EDE}_{k_2}, \ldots, \mathrm{EDE}_{k_n}\right\}$$
$$\mathrm{CDF}^* = \left\{ \frac{k_i}{\|\mathrm{EDEs}^*\|} \middle| i \in \{1, 2, \ldots, n\} \right\} \tag{30}$$

where n : time steps of each scenario

$$\left\|\mathrm{EDE}_{k_1}\right\| \leq \left\|\mathrm{EDE}_{k_2}\right\| \leq \cdots \leq \left\|\mathrm{EDE}_{k_n}\right\|$$

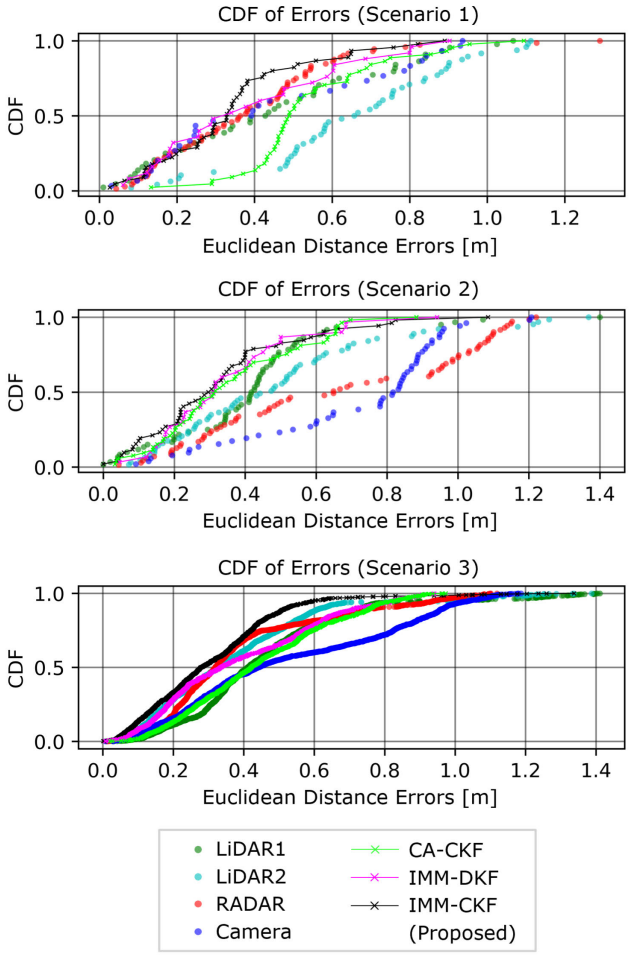

FIGURE 13. CDF comparison for three scenarios.

The CDF results for the three scenarios in Fig. 9 are shown in Fig. 13. In the graphs of Fig. 13, the x-axis and y-axis represent EDEs* and CDF*, respectively. According to (30), the smaller the mean error, the more the graph is shifted to the left. In all three graphs in Fig. 13, the proposed method, IMM-CKF, is shifted the farthest to the left, indicating the smallest errors. Therefore, it is shown that the proposed method outperforms the reference algorithms and individual sensors in terms of the performance.

Further experiments were conducted to validate the performance in the same scenarios with sensor failures. The sensor fusion results with the remaining two sensors are presented in Table. 2. Three test cases for two-sensor fusions (assuming the other two sensors failed) were conducted to to compare centralized fusion with distributed fusion. The fusion results with RADAR and LiDAR 1 show similar tracking performance in both fusion algorithms. This indicates that the performance improvement of IMM-CKF is not noticeable when the camera data is excluded, and rather IMM-DKF performs slightly better. However, when camera data is available in two sensor combinations, the proposed method outperforms other methods. The camera

TABLE 1. Accuracy comparison of various methods.

	Sensor/Algorithm	ARMSE [m]
Sensor	RADAR	0.3935
	Camera	0.6515
	LiDAR1	0.4486
	LiDAR2	0.4231
Sensor fusion algorithm	CA-CKF	0.4572
	IMM-DKF	0.3913
	IMM-CKF (Proposed)	**0.3461**

measurements often induce large errors in the longitudinal direction but are accurate in the lateral direction. Therefore, IMM-CKF can set parameters of longitudinal uncertainty to a high value such that the lateral information is mainly fused with other sensor data during state updates. However, in the distributed framework, the longitudinal uncertainty cannot be set high because the structure has to track the object using only camera data in its sub-filter. As a result, the camera sensor degrades the performance of the IMM-DKF. The proposed method can overcome the limitation of distributed one and demonstrates consistent performance across scenarios with sensor failures.

An additional test was conducted to validate the capability of maintaining track continuity in the event of sequential multiple sensor failures. Four test cases for single sensor perception (assuming the other three sensors failed) were performed to analyze track continuity performance when the TV made multiple lane changes. Several sensor signals have been blocked sequentially as shown in Table. 3 by assuming bad weather or harsh environment. At a specific time interval, only one sensor data is available with other sensor signals blocked. The experimental results are illustrated in Fig. 14 and three regions are enlarged to compare the continuity performance of the sensor fusion methods. The results from the IMM-DKF lose its continuity due to its structural limitations. Any discontinuity should be avoided because discontinuous tracking causes a significant shift in the track's position. In contrast, IMM-CKF and CA-CKF preserve the continuity of the track state with some errors while switching among four sensor measurements.

B. EVALUATION OF THE PROPOSED IMM FILTER AND THE TRACK COMPENSATION

In this section, the proposed centralized IMM filter and the track compensation algorithm are evaluated from the tracking perspectives. The speed and yaw estimation results are compared between IMM-CKF and CA-CKF. The CA model is commonly utilized for object tracking in the moving reference frame, and the state vector is defined as relative values. Since the results from CA-CKF has relative quantities, the speed of the track is obtained by adding its relative speed to the HV's speed.

To verify the performance of track compensation, three test cases were performed for TVs driving on straight road,

TABLE 2. Accuracy comparison with two sensor fusions.

Available sensors	Method	ARMSE [m]
RADAR and LiDAR1	CA-CKF	0.4132
	IMM-DKF	**0.3982**
	IMM-CKF (Proposed)	0.4017
Camera and LiDAR1	CA-CKF	0.6138
	IMM-DKF	0.5493
	IMM-CKF (Proposed)	**0.3657**
Camera and RADAR	CA-CKF	0.5871
	IMM-DKF	0.5162
	IMM-CKF (Proposed)	**0.3918**

TABLE 3. Sensor failure test case.

Time [s]	Available sensor
$0 \sim 8$	RADAR only
$8 \sim 14$	Camera only
$14 \sim 23$	LiDAR1 only
$23 \sim 29$	LiDAR2 only

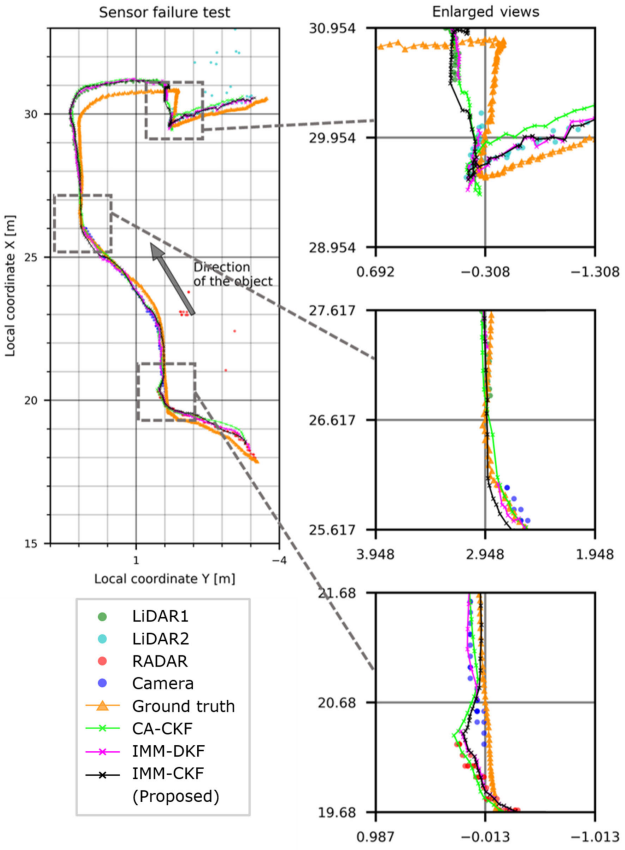

FIGURE 14. Tracking results with sensor failures.

curved road, and stationary TV. Their tracking results on straight and curved roads are illustrated in Fig. 15 and Fig. 16, respectively. Because the HV is following the TV, speed estimation results from both methods are similar. However, the estimated yaw angle and yaw rate show large

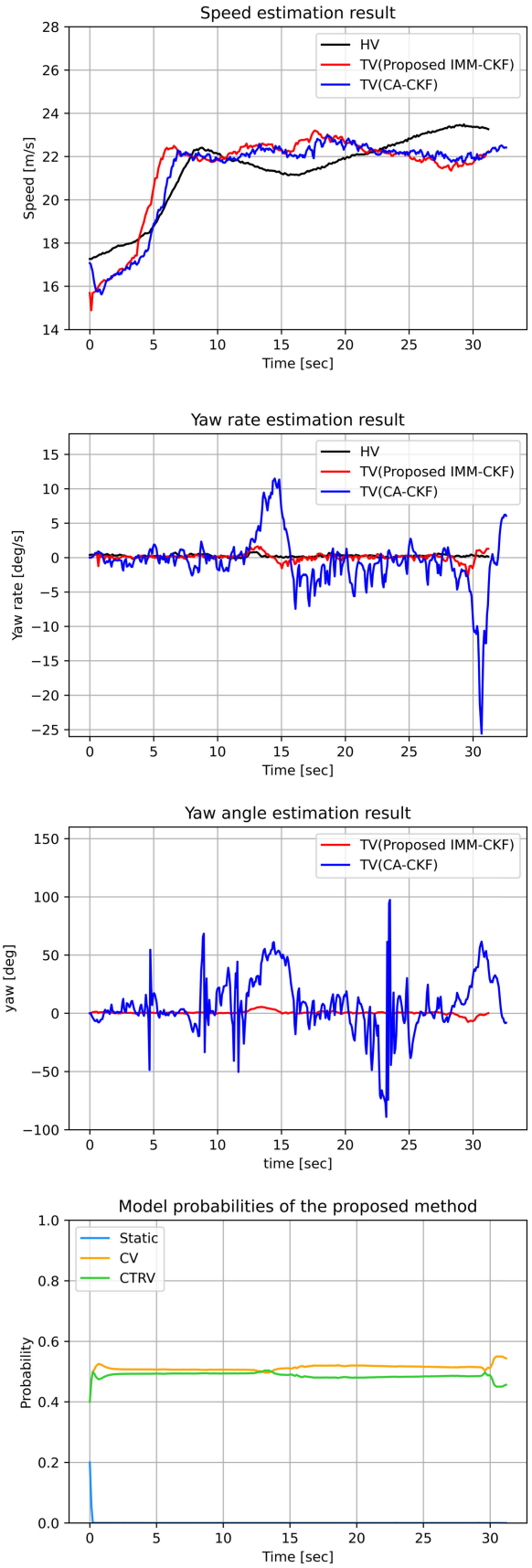

FIGURE 15. Evaluation of the proposed IMM filter and the track compensation: straight road scenario.

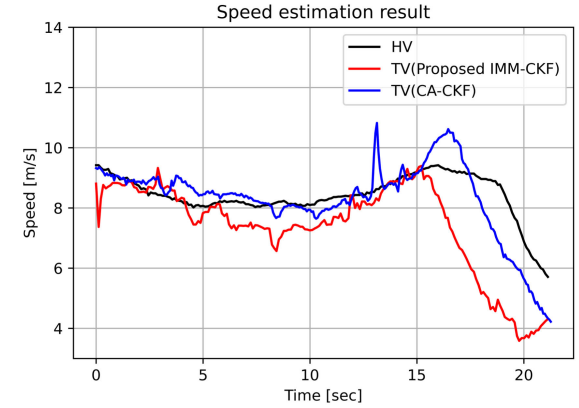

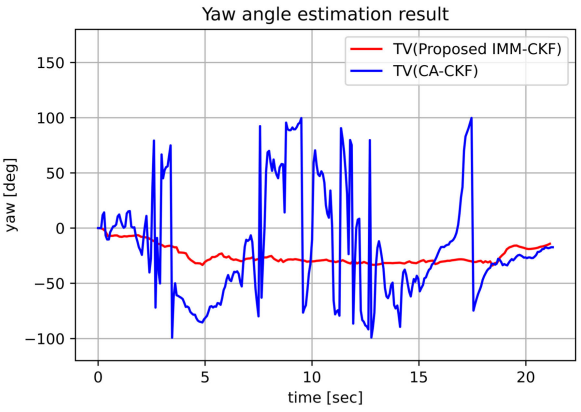

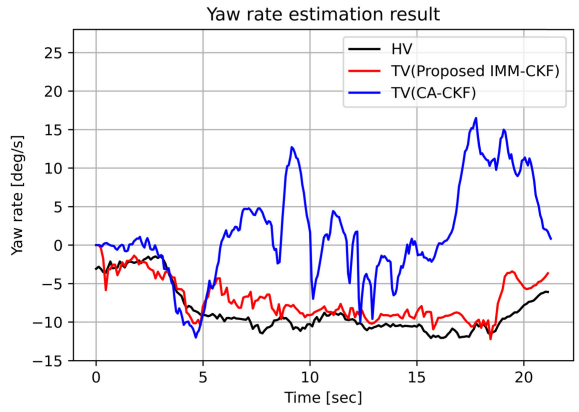

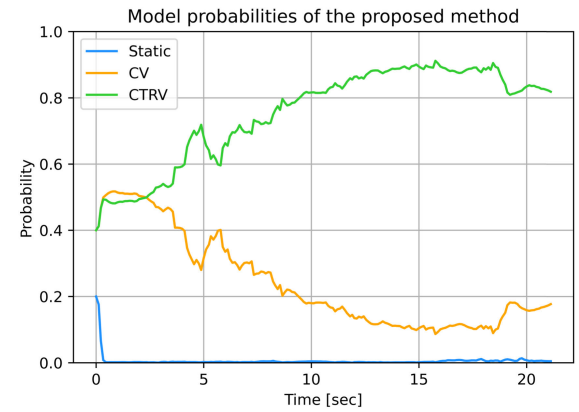

FIGURE 16. Evaluation of the proposed IMM filter and the track compensation: constant turning scenario.

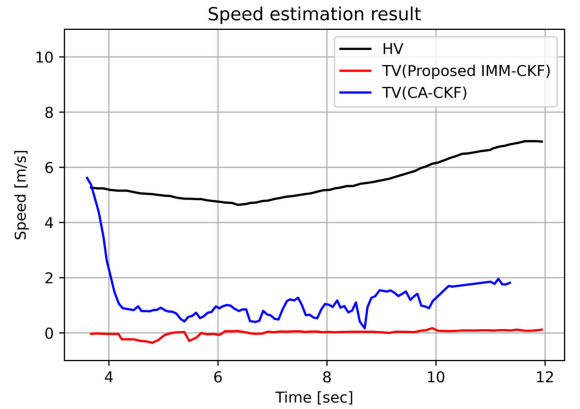

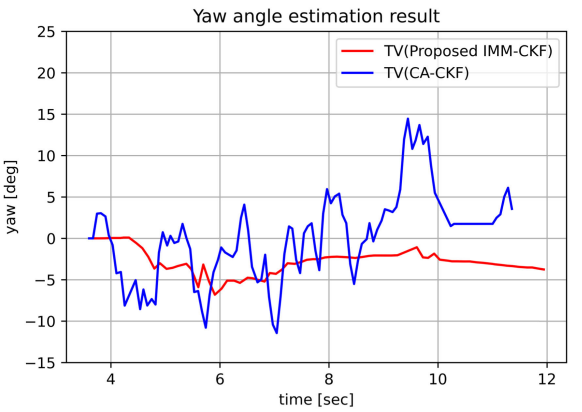

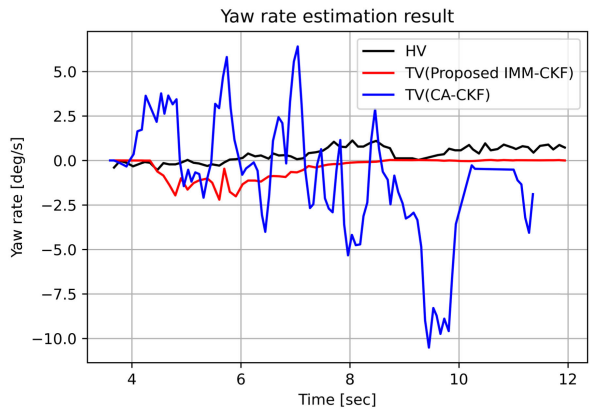

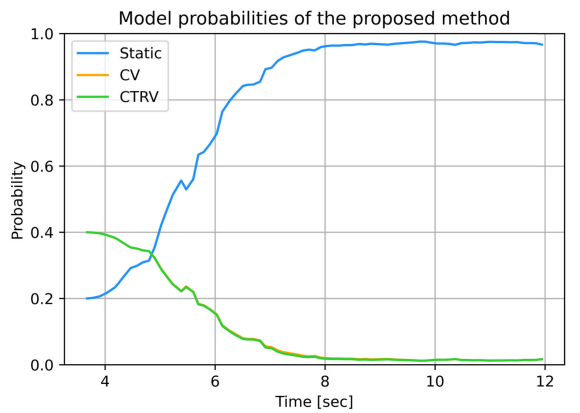

FIGURE 17. Evaluation of the proposed IMM filter and the track compensation: stationary object scenario.

errors with CA-CKF on both experiments. The CA-CKF determines the yaw angle from the ratio of the longitudinal speed and the lateral speed. Thus, the CA-CKF shows limitations in providing the information of the actual motion of the object. On the other hand, the proposed method estimates the object's speed and yaw angle/rate correctly using the track compensation algorithm. When the yaw rate becomes 0, the CTRV model is equivalent to the CV model, thus, as illustrated in the last graph of Fig. 15, the mode probabilities of the two models remain at similar values.

When the HV and the TV are traveling on the same curved road, only the proposed method indicates that the HV and the TV are turning with the similar yaw rate as illustrated in the third graph of Fig. 16. In addition, reflecting the motion of a vehicle along a curved road, the mode probability of the CTRV model is greater than other models as shown in the last graph of Fig. 16. This indicates that the proposed track compensation can handle the tracking problem in a moving reference frame, and the proposed algorithm can compute the actual speed and yaw rate of objects accurately.

Another experiment was conducted to detect the stationary TV on the road as shown in Fig. 17. With the CA-CKF, TV's yaw angle is estimated with large errors even with backward direction. This is because the HV is in motion, TV is perceived as if it is in motion in the moving reference frame. However, with the proposed IMM filter and the track compensation method, the tracking of the stationary object is correctly achieved with almost zero speed, yaw angle, and yaw rate. The last graph of Fig. 17 indicates the highest mode probability on the static model compared with other models.

VI. CONCLUSION

In this paper, a robust multi-sensor object tracking system is proposed through two steps. First, A novel centralized Interacting Multiple Model (IMM) filter is presented to fuse measurements from multiple sensors through one central filter. The proposed IMM is integrated with the Centralized Kalman Filter (CKF) so that it provides optimal estimates over heterogeneous measurements. The proposed IMM filter can be implemented to multi-sensor systems by modifying the mode probability of the original IMM. Secondly, to address a tracking problem in a moving reference frame, a track compensation algorithm is proposed to estimate the actual motion of an object only using in-vehicle sensor data. With the compensation, the estimation performance is not affected by either localization qualities or global positioning sensor failures. Several experimental scenarios are conducted to verify the proposed method. The proposed method maintains track continuity even when sensors fail or asynchronous measurements occur due to its structure. Experimental results demonstrate that the proposed method outperform individual sensor output and the baseline methods. In addition, the results indicate that the actual motion of an object is appropriately estimated when tracking in the reference moving frame.

REFERENCES

[1] *Taxonomy and Definitions for Terms Related to Driving Automation Systems for On-Road Motor Vehicles*, On-Road Automated Driving (ORAD) Committee, SAE Int., Warrendale, PA, USA, 2021.

[2] F. Castanedo, "A review of data fusion techniques," *Sci. World J.*, vol. 2013, pp. 1–19, Oct. 2013.

[3] Z. Wang, Y. Wu, and Q. Niu, "Multi-sensor fusion in automated driving: A survey," *IEEE Access*, vol. 8, pp. 2847–2868, 2020.

[4] M. B. Alatise and G. P. Hancke, "A review on challenges of autonomous mobile robot and sensor fusion methods," *IEEE Access*, vol. 8, pp. 39830–39846, 2020.

[5] P. Kolar, P. Benavidez, and M. Jamshidi, "Survey of datafusion techniques for laser and vision based sensor integration for autonomous navigation," *Sensors*, vol. 20, no. 8, p. 2180, Apr. 2020.

[6] M. Khodarahmi and V. Maihami, "A review on Kalman filter models," *Arch. Comput. Methods Eng.*, vol. 30, no. 1, pp. 727–747, Jan. 2023.

[7] D. J. Yeong, G. Velasco-Hernandez, J. Barry, and J. Walsh, "Sensor and sensor fusion technology in autonomous vehicles: A review," *Sensors*, vol. 21, no. 6, p. 2140, Mar. 2021.

[8] R. E. Kalman, "A new approach to linear filtering and prediction problems," *J. Basic Eng.*, vol. 82, no. 1, pp. 35–45, Mar. 1960.

[9] H. A. P. Blom and Y. Bar-Shalom, "The interacting multiple model algorithm for systems with Markovian switching coefficients," *IEEE Trans. Autom. Control*, vol. AC-33, no. 8, pp. 780–783, Aug. 1988.

[10] E. Mazor, A. Averbuch, Y. Bar-Shalom, and J. Dayan, "Interacting multiple model methods in target tracking: A survey," *IEEE Trans. Aerosp. Electron. Syst.*, vol. 34, no. 1, pp. 103–123, 1998.

[11] D. Ruppert and M. P. Wand, "Multivariate locally weighted least squares regression," *Ann. Statist.*, vol. 22, no. 3, pp. 1346–1370, Sep. 1994.

[12] F. Gustafsson, *Statistical Sensor Fusion*. Studentlitteratur, Lund, Sweden, 2010.

[13] H. Ma, L. Yan, Y. Xia, and M. Fu, *Kalman Filtering and Information Fusion*. Singapore: Springer, 2020.

[14] N. E. ElHady and J. Provost, "A systematic survey on sensor failure detection and fault-tolerance in ambient assisted living," *Sensors*, vol. 18, no. 7, p. 1991, Jun. 2018.

[15] S. U. Jan, Y. D. Lee, and I. S. Koo, "A distributed sensor-fault detection and diagnosis framework using machine learning," *Inf. Sci.*, vol. 547, pp. 777–796, Feb. 2021.

[16] C. Sun and Y. Lin, "Adaptive output feedback compensation for a class of nonlinear systems with actuator and sensor failures," *IEEE Trans. Syst., Man, Cybern., Syst.*, vol. 52, no. 8, pp. 4762–4771, Aug. 2022.

[17] F. De Ponte Müller, "Survey on ranging sensors and cooperative techniques for relative positioning of vehicles," *Sensors*, vol. 17, no. 2, p. 271, Jan. 2017.

[18] K. Jo, M. Lee, and M. Sunwoo, "Track fusion and behavioral reasoning for moving vehicles based on curvilinear coordinates of roadway geometries," *IEEE Trans. Intell. Transp. Syst.*, vol. 19, no. 9, pp. 3068–3075, Sep. 2018.

[19] Y. Luo, Y. Liao, Z. Li, K. Zhang, and H. Wang, "Radar target tracking based on interactive multi-model cubature Kalman filter," in *Proc. 7th Int. Conf. Comput. Commun. Syst. (ICCCS)*, Apr. 2022, pp. 452–457.

[20] P. Dahal, S. Mentasti, S. Arrigoni, F. Braghin, M. Matteucci, and F. Cheli, "Extended object tracking in curvilinear road coordinates for autonomous driving," *IEEE Trans. Intell. Vehicles*, vol. 8, no. 2, pp. 1266–1278, Feb. 2023.

[21] I. Arasaratnam and S. Haykin, "Cubature Kalman filters," *IEEE Trans. Autom. Control*, vol. 54, no. 6, pp. 1254–1269, Jun. 2009.

[22] D. Wang, H. Lv, and J. Wu, "Augmented cubature Kalman filter for nonlinear RTK/MIMU integrated navigation with non-additive noise," *Measurement*, vol. 97, pp. 111–125, Feb. 2017.

[23] R. Havangi, "Adaptive robust unscented Kalman filter with recursive least square for state of charge estimation of batteries," *Electr. Eng.*, vol. 104, no. 2, pp. 1001–1017, Apr. 2022.

[24] S. Yazdkhasti, D. Sabzevari, and J. Z. Sasiadek, "Adaptive H-infinity extended Kalman filtering for a navigation system in presence of high uncertainties," *Trans. Inst. Meas. Control*, vol. 45, no. 8, pp. 1430–1442, May 2023.

[25] M. Kolat, O. Törő, and T. Bécsi, "Performance evaluation of a maneuver classification algorithm using different motion models in a multi-model framework," *Sensors*, vol. 22, no. 1, p. 347, Jan. 2022.

[26] H. P. Blom, "An efficient filter for abruptly changing systems," in *Proc. 23rd IEEE Conf. Decis. Control*, Dec. 1984, pp. 656–658.

[27] J. Zubaca, M. Stolz, R. Seeber, M. Schratter, and D. Watzenig, "Innovative interaction approach in IMM filtering for vehicle motion models with unequal states dimension," *IEEE Trans. Veh. Technol.*, vol. 71, no. 4, pp. 3579–3594, Apr. 2022.
[28] Y. Li and C. Bian, "Object tracking in satellite videos: A spatial–temporal regularized correlation filter tracking method with interacting multiple model," *IEEE Geosci. Remote Sens. Lett.*, vol. 19, pp. 1–5, 2022.
[29] W. Wenkang, F. Jingan, S. Bao, and L. Xinxin, "Vehicle state estimation using interacting multiple model based on square root cubature Kalman filter," *Appl. Sci.*, vol. 11, no. 22, p. 10772, Nov. 2021.
[30] J. Lim, H.-S. Kim, and H.-M. Park, "Interactive-multiple-model algorithm based on minimax particle filtering," *IEEE Signal Process. Lett.*, vol. 27, pp. 36–40, 2020.
[31] Y. Liu, Z. Wang, L. Peng, Q. Xu, and K. Li, "A detachable and expansible multisensor data fusion model for perception in level 3 autonomous driving system," *IEEE Trans. Intell. Transp. Syst.*, vol. 24, no. 2, pp. 1814–1827, Feb. 2023.
[32] R. Gravina, P. Alinia, H. Ghasemzadeh, and G. Fortino, "Multi-sensor fusion in body sensor networks: State-of-the-art and research challenges," *Inf. Fusion*, vol. 35, pp. 68–80, May 2017.
[33] R. Olfati-Saber, "Distributed Kalman filter with embedded consensus filters," in *Proc. 44th IEEE Conf. Decis. Control*, Dec. 2005, pp. 8179–8184.
[34] S. P. Talebi and S. Werner, "Distributed Kalman filtering and control through embedded average consensus information fusion," *IEEE Trans. Autom. Control*, vol. 64, no. 10, pp. 4396–4403, Oct. 2019.
[35] D.-J. Xin, L.-F. Shi, and X. Yu, "Distributed Kalman filter with faulty/reliable sensors based on Wasserstein average consensus," *IEEE Trans. Circuits Syst. II, Exp. Briefs*, vol. 69, no. 4, pp. 2371–2375, Apr. 2022.
[36] K. Yoon, J. Choi, and K. Huh, "Adaptive decentralized sensor fusion for autonomous vehicle: Estimating the position of surrounding vehicles," *IEEE Access*, vol. 11, pp. 90999–91008, 2023.
[37] K. Cai, T. Qu, H. Chen, B. Gao, and N. Bian, "Low-cost hybrid multisensor fusion method and implementation for production intelligent vehicles," *IEEE Trans. Instrum. Meas.*, vol. 71, pp. 1–16, 2022.
[38] L. Hong-Tao and K. Feng-Ju, "Tracking UUV based on interacting multiple model unscented particle filter with multi-sensor information fusion," *Optik*, vol. 126, no. 24, pp. 5067–5073, Dec. 2015.
[39] M. Cen, X. Liu, and D. Luo, "Multi-sensor IMM estimator for uncertain measurement," in *Proc. 5th Int. Conf. Wireless Commun., Netw. Mobile Comput.*, Sep. 2009, pp. 1–4.
[40] C. Zhifeng, C. Yunze, and X. Xiaoming, "A data fusion algorithm for multi-sensor dynamic system based on interacting multiple model," in *Proc. 31st Chin. Control Conf.*, Jul. 2012, pp. 199–203.
[41] T. Cho, C. Lee, and S. Choi, "Multi-sensor fusion with interacting multiple model filter for improved aircraft position accuracy," *Sensors*, vol. 13, no. 4, pp. 4122–4137, Mar. 2013.
[42] C. Yang, A. Mohammadi, and Q.-W. Chen, "Multi-sensor fusion with interaction multiple model and chi-square test tolerant filter," *Sensors*, vol. 16, no. 11, p. 1835, Nov. 2016.
[43] Q. Shen, J. Liu, X. Zhou, W. Qin, L. Wang, and Q. Wang, "Centralized fusion methods for multi-sensor system with bounded disturbances," *IEEE Access*, vol. 7, pp. 141612–141626, 2019.
[44] S. F. Kara and B. Basaran, "An application of IMM based sensor fusion algorithm in train positioning system," in *Proc. IEEE Int. Conf. Multisensor Fusion Integr. Intell. Syst. (MFI)*, Sep. 2020, pp. 249–254.
[45] J. Qiu, Z. Xing, C. Zhu, K. Lu, J. He, Y. Sun, and L. Yin, "Centralized fusion based on interacting multiple model and adaptive Kalman filter for target tracking in underwater acoustic sensor networks," *IEEE Access*, vol. 7, pp. 25948–25958, 2019.
[46] L. Wang and S. Li, "Enhanced multi-sensor data fusion methodology based on multiple model estimation for integrated navigation system," *Int. J. Control, Autom. Syst.*, vol. 16, no. 1, pp. 295–305, Feb. 2018.
[47] Y. Yang and H. Zuo, "Multi-sensor fusion estimation algorithm based on IMM and SCC," in *Proc. 4th Int. Conf. Artif. Intell. Electromechanical Autom. (AIEA)*, Oct. 2023, pp. 524–533.
[48] R. Altendorfer, "Observable dynamics and coordinate systems for automotive target tracking," in *Proc. IEEE Intell. Vehicles Symp.*, Jun. 2009, pp. 741–746.
[49] W. Farrell, "Interacting multiple model filter for tactical ballistic missile tracking," *IEEE Trans. Aerosp. Electron. Syst.*, vol. 44, no. 2, pp. 418–426, Apr. 2008.
[50] J. Chen, Y. Zhang, Y. Yang, and C. Qu, "Multi-target track-to-track association based on relative coordinate assignment matrix," in *Proc. 33rd Chin. Control Decis. Conf. (CCDC)*, May 2021, pp. 1255–1260.
[51] K. Jo, M. Lee, J. Kim, and M. Sunwoo, "Tracking and behavior reasoning of moving vehicles based on roadway geometry constraints," *IEEE Trans. Intell. Transp. Syst.*, vol. 18, no. 2, pp. 460–476, Feb. 2017.
[52] D. Svensson, "Derivation of the discrete-time constant turn rate and acceleration motion model," in *Proc. Sensor Data Fusion, Trends, Solutions, Appl. (SDF)*, Oct. 2019, pp. 1–5.
[53] R. M. A. Ikram, L. Goliatt, O. Kisi, S. Trajkovic, and S. Shahid, "Covariance matrix adaptation evolution strategy for improving machine learning approaches in streamflow prediction," *Mathematics*, vol. 10, no. 16, p. 2971, Aug. 2022.
[54] Z. T. Ke, Y. Ma, and X. Lin, "Estimation of the number of spiked eigenvalues in a covariance matrix by bulk eigenvalue matching analysis," *J. Amer. Stat. Assoc.*, vol. 118, no. 541, pp. 374–392, Jan. 2023.
[55] S. Thrun, "Probabilistic robotics," *Commun. ACM*, vol. 45, no. 3, pp. 52–57, 2002.
[56] B. Ristic, S. Arulampalam, and N. Gordon, *Beyond the Kalman Filter: Particle Filters for Tracking Applications*. Norwood, MA, USA: Artech House, 2003.
[57] N. Brouwer, H. Kloeden, and C. Stiller, "Comparison and evaluation of pedestrian motion models for vehicle safety systems," in *Proc. IEEE 19th Int. Conf. Intell. Transp. Syst. (ITSC)*, Nov. 2016, pp. 1–6.
[58] Z. Duan, C. Han, and T. Tao, "Optimal multi-sensor fusion target tracking with correlated measurement noises," in *Proc. IEEE Int. Conf. Syst., Man Cybern.*, Oct. 2004, pp. 1272–1278.
[59] L. A. Johnston and V. Krishnamurthy, "An improvement to the interacting multiple model (IMM) algorithm," *IEEE Trans. Signal Process.*, vol. 49, no. 12, pp. 2909–2923, 2001.
[60] K. Jo, K. Chu, and M. Sunwoo, "Interacting multiple model filter-based sensor fusion of GPS with in-vehicle sensors for real-time vehicle positioning," *IEEE Trans. Intell. Transp. Syst.*, vol. 13, no. 1, pp. 329–343, Mar. 2012.
[61] K. B. Athreya and S. N. Lahiri, *Measure Theory and Probability Theory*, vol. 19. New York, NY, USA: Springer, 2006.

JAEHO CHOI received the B.S. degree in automotive engineering from Kookmin University, Seoul, South Korea, in 2017. He is currently pursuing the Ph.D. degree with the Department of Automotive Engineering (Automotive-Computer Convergence). His research interests include the LiDAR data processing and the high-level fusion. He has been aiming for increment perception performance through sensor fusion and machine learning for autonomous vehicles.

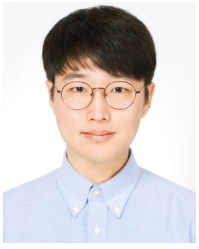

JONGWON PARK received the B.S. degree in mechanical engineering from Hanyang University, Seoul, Republic of Korea, in 2013, and the Ph.D. degree from the Department of Automotive Engineering, Hanyang University, South Korea. His research interests include vehicle chassis control, autonomous driving, sensor fusion, and deep learning.

KUNSOO HUH (Member, IEEE) received the Ph.D. degree from the University of Michigan, Ann Arbor, MI, USA, in 1992. He is currently a Professor with the Department of Automotive Engineering, Hanyang University, Seoul, South Korea. His research interest includes machine monitoring and control, with emphasis on their applications to vehicular systems. His current research interests include sensor-based active safety systems, V2X-based safety systems, autonomous vehicle control, and AI applications in autonomous vehicle.